# Formation of Poly(1,1,2,2-tetrahydroperfluorodecyl acrylate) Submicron Fibers and Particles from Supercritical Carbon Dioxide Solutions

**Simon Mawson,† Keith P. Johnston,*,† James R. Combes,‡ and Joseph M. DeSimone‡**

*Department of Chemical Engineering, University of Texas, Austin, Texas 78712, and Department of Chemistry, University of North Carolina, Chapel Hill, North Carolina 27599-3290*

*Received September 26, 1994; Revised Manuscript Received February 20, 1995®*

ABSTRACT: Rapid expansion from supercritical solution (RESS) of a crystalline fluoropolymer, poly(1,1,2,2-tetrahydroperfluorodecyl acrylate) or poly(TA-N), in carbon dioxide produces submicron to several micron sized particles and fibers. The understanding of the RESS mechanism has been clarified by careful design of experimental variables and procedures. The concentration of the poly(TA-N)/$CO_2$ solution was held constant (at 0.5 and 2.0 wt %), the solution cloud point curves were obtained, the pre-expansion temperature was varied above and below the cloud point, and the length to diameter (*L/D*) ratio of the nozzle was varied from 8.5 to 508. The morphology is explained in terms of the location of phase separation within the expansion nozzle. The *L/D* is the most influential variable for achieving a transition from particles or fibers. In most cases, manipulation of the solution concentration and the pre-expansion temperature did not produce this transition but did have a large effect on the sizes of the particles and fibers. These results are an important step in demonstrating $CO_2$-based spray processes which do not require any volatile organic solvents.

## Introduction

A variety of organic and inorganic powders and fibers have been produced by rapid expansion from supercritical solution (RESS).[1–11,18] In RESS, the mechanical perturbation which occurs when a solution is expanded across a fine throttling device, such as a capillary or orifice nozzle, can lead to a rapid supersaturation, with characteristic times for phase separation between $10^{-5}$ and $10^{-7}$ s.[8,9] Consequently, microstructural materials may be formed and quenched in the rapidly expanding solution. Examples of morphologies of crystalline and amorphous polymers include 0.3–7.0 μm fibers,[6,8,10,11] 0.2–5.0 μm spherical particles,[6,8,10] encapsulated drug delivery systems,[7,18] and metastable nonequilibrium blends[8,9] (see Table 1).

RESS has been modeled with classical nucleation theory[12–14] and a surface energy model developed by Liang et al.[15] Lele and Shine[6] offered a theoretical and conceptual framework for predicting whether fibers or particles are produced by RESS. Precipitation early in the nozzle leads to fibers, since there is a long time ($10^1$ s) for growth of the polymer-rich domains, which are then sheared into fibers. This "long time" precipitation mode is likely when the solution entering the nozzle is near the phase boundary or in a two-phase region. In contrast, fine particles are produced if the solution precipitates near the end of the nozzle or in the free jet. This mode is likely when a homogeneous solution starts far from the phase boundary, since the time for growth is greatly diminished ($10^{-6}$ s). Factors which influence the phase behavior and thus the characteristic time for particle growth and fiber formation depend upon the pre-expansion temperature, pressure, solute concentration, and the length to diameter, *L/D*, in the expansion nozzle.

To date, most studies of RESS of polymers have not determined the solution phase behavior. For semicrystalline polymers, both fluid–solid and fluid–liquid phase separation mechanisms are possible.[16] The type of phase behavior and the proximity to the phase boundaries during RESS may be expected to have a profound effect on the morphology. Another limitation is that the concentration of the polymer dissolved by the flowing solvent has often been unknown (see Table 1). Also, the *L/D* has usually been constant or varied over a small range, although Tom et al.[18] have recently shown a particle to fiber transition for poly(L-lactic acid) by varying the *L/D* for a 30 μm capillary from 167 to 500. Therefore, it has been difficult to achieve a fundamental understanding of how the various morphologies are produced. The purpose of this study is to overcome these experimental limitations by obtaining phase equilibria data and by performing RESS under well-defined conditions over a wide range of *L/D*. Very recently, Lele and Shine[8] reported a new experimental procedure for RESS in which the pre-expansion concentration was somewhat controlled, with a 30% depletion in concentration occurring after spraying the solution for 20 min. Furthermore, phase equilibria data were reported. This study was quite successful in demonstrating their conceptual framework described above.

The majority of RESS studies of polymers have used organic solvents, such as $C_1$–$C_5$ alkanes and alkenes, as well as chlorofluorocarbons (CFCs). In supercritical fluid technology, great effort is underway to attempt to replace these types of solvents with $CO_2$.[19–25] $CO_2$ is nontoxic, nonflammable, and environmentally acceptable and has easily accessible critical conditions, i.e., $T_c = 31$ °C and $P_c = 73.8$ bar. It has no dipole moment and a low cohesive energy density. Therefore, for pressures up to 200 bar, only very low molecular weight polymers are soluble in $CO_2$, e.g., poly(dimethysiloxane)s, atactic polypropylene, and polymethacrylates with large hydrocarbon branches.[26]

† University of Texas.
‡ University of North Carolina.
® Abstract published in *Advance ACS Abstracts,* April 1, 1995.

0024-9297/95/2228-3182$09.00/0 

**Table 1. Polymers Precipitated at Various RESS Operating Conditions Using a Variety of Supercritical Solvents**

| polymer | solvent | *L/D* | $T_{pre}$ (°C) | press. (bar) | conc (wt %) | morphology |
|---|---|---|---|---|---|---|
| polystyrene (PS) | pentane[2,10] | 200 | 200–350 | 170 | NR[a] | spheres/fibers |
| polypropylene | pentane[2,10] | 200 | 200–400 | 170 | NR | fibers |
| | pentane[11] | 120–1200 | 225 | 170 | NR | fibers |
| cellulose acetate | pentane[11] | 200 | 230 | 170 | NR | fibers |
| poly(carbosilane) | pentane[2,10] | 200 | 200–400 | 170–238 | NR | particles/fibers |
| poly(phenylsulfone) | propane[2,10] | 200 | 150 | 170 | NR | spheres |
| poly(methyl methacrylate) | propane[2,10] | 200 | 125–300 | 170 | NR | fibers |
| | CDFM[6] | 5.1–8.5 | 110–130 | 82.7–207 | NR | particles/fibers |
| poly(1-butene) | $CO_2$[27] | 187.5 | 130 | 550 | NR | spheres |
| poly(ethylene succinate) | $CO_2$[27] | 187.5 | 40 | 275 | NR | spheres |
| poly(caprolactone) | $CO_2$[27] | 187.5 | 40–90 | 412 | NR | spheres |
| | CDFM[6,8] | 6.4–12.7 | 110–130 | 159–310 | 0.078–0.310 | particles/fibers |
| poly(L-lactic acid) | $CO_2$[7] | 10 | 45–65 | 200–300 | 0.013–0.074 | particles/spheres |
| | $CO_2$/CDFM[18] | 500 | 80–120 | 210 | NR | spheres/dendrites |
| | CDFM[6,8] | 7.7–8.5 | 110–150 | 152–345 | 0.080 | particles/fibers |
| PS–PMMA copolymer | CDFM[6,8,9] | 5.1 | 110 | 159–276 | 0.051–0.080 | particles/fibers |
| poly(ethyl methacrylate) | CDFM[8,9] | 7.7 | 90–110 | 207–276 | 0.080 | particle/fiber blend |
| PMMA–PEMA blends | CDFM[8,9] | 7.7–8.5 | 90–130 | 159–276 | 0.051–0.080 | particles/fibers |
| poly(TA-N) | $CO_2$ | 8.5/508 | 30–105 | 207 | 0.5/2.0 | particles/fibers |

[a] Not reported.

A few attempts have been made to use $CO_2$ for RESS of polymers (see Table 1). For example, Lele and Shine[27] studied the semicrystalline polymers poly(1-butene), poly(ethylene succinate), poly(caprolactone), and poly(hexamethylene sebacate). However, size exclusion chromatography revealed that only the lowest molecular weight oligomers were soluble in $CO_2$ at pressures ranging from 275 to 550 bar. In addition, solution concentrations were not reported. Tom et al.[28] used $CO_2$ to produce submicron biodegradable polymer particles for encapsulated drug delivery systems including poly(L-lactic acid) (L-PLA), poly(DL-lactic acid), and poly(glycolic acid). Initial solubility of the L-PLA in carbon dioxide was 0.14 wt % but rapidly dropped off to less than 0.05 wt % once the lowest MW oligomers had been extracted. With the addition of 27 wt % chlorodifluoromethane as a cosolvent, the solubility only increased by a factor of 2–4.[18]

Because so many polymers are not highly soluble in $CO_2$, $CO_2$ may be used as an antisolvent to form microstructural materials. Polymer solutions in solvents such as toluene and dimethylformamide may be sprayed through 30–200 $\mu$m nozzles into gaseous, liquid, or supercritical $CO_2$ to form 100 nm particles,[29,30] highly oriented microfibrils,[31,32] bicontinuous networks,[30] solid and hollow fibers with porous shells,[30,32,33] encapsulated drug delivery system,[34] and 100 nm microballoons with porous shells.[30,35] Although the phase separation caused by two-way mass transfer is much slower than that caused by pressure reduction in RESS,[9] the sizes of the particles and fibers are similar in the two processes. Thus, it should be possible to improve RESS to achieve faster expansion and smaller products.

In yet another spray process, $CO_2$ is used to replace the fast-evaporating volatile organic solvent in spray-coating applications.[36] Although the volatile organic carbon emissions are reduced up to 2/3, some organic solvent is still required due to the lack of solubility of most polymers in $CO_2$. A goal of the present study is to spray polymer solutions in $CO_2$ without any organic solvents.

Fluoropolymers are often highly soluble in $CO_2$, especially fluorinated acrylic polymers, such as poly(1,1-dihydroperfluorooctyl acrylate) or poly(FOA). This fluoropolymer can be homogeneously synthesized in $CO_2$ up to at least 70% solids at 65 °C and 345 bar.[21] Recently, it was shown that PMMA with a degree of polymerization (DP) >3000 could be synthesized in $CO_2$ by dispersion polymerization by using a poly(FOA) stabilizer.[37]

In this study, we investigate the feasibility of using $CO_2$ as a solvent for producing submicron fibers and particles of an appreciably soluble fluoropolymer, poly(1,1,2,2-tetrahydroperfluorodecyl acrylate) or poly(TA-N). The fluorocarbon side chain is crystalline unlike the case for poly(FOA). We perform carefully controlled RESS experiments with a known and constant inlet concentration to better understand the mechanisms which describe the morphology and to provide a well-defined data base for theoretical modeling. The phase behavior is investigated, as it is instrumental for building a foundation to understand the mechanism. In order to manipulate the phase separation and the formation of product, we vary the concentration of the fluoropolymer and the pre-expansion temperature in a systematic fashion. The pre-expansion temperature is varied below and above both the melting point of poly(TA-N) and the cloud point temperature of the solution. The highest solution concentration, 2.0 wt %, is well above that in most previous RESS studies, due to the high solubility of the polymer in $CO_2$. The length to diameter, *L/D*, of the expansion nozzle will be varied from 8.5 to 508 to attempt to demonstrate a transition from particles to fibers and to understand the expansion mechanism.

## Experimental Section

**Equipment.** The experimental apparatus for both phase equilibria measurements and RESS is shown in Figure 1. The stainless steel variable-volume view cell contained a sapphire window, 1 in. in diameter and 3/8 in. thick, as reported previously.[38] Because a piston isolated a polymer solution of known concentration from the pressurizing fluid (pure $CO_2$), the mole fraction of the polymer was constant. The entire cell assembly was placed in a polycarbonate water bath and the temperatures controlled to within ±0.1 °C using a Polystat water circulator. The pressurizing fluid for the piston was $CO_2$. Carbon dioxide was compressed with a Haskel air-driven gas booster (Model AC-152) and stored in a 300 mL high-pressure reservoir. It was metered into a manual syringe pump (60 $cm^3$, High Pressure Equipment Co., Model 87-65) using a Tescom pressure regulator (Model 26-1021). The fluid pressure in the syringe pump was monitored with a Sensotec digital pressure transducer (TJE/7039-01) to within ±0.2 bar. For the static phase equilibria experiments, the syringe pump was used to control the piston pressure. However, in RESS experiments, the pressure on the backside of the piston was controlled with the pressure regulator.

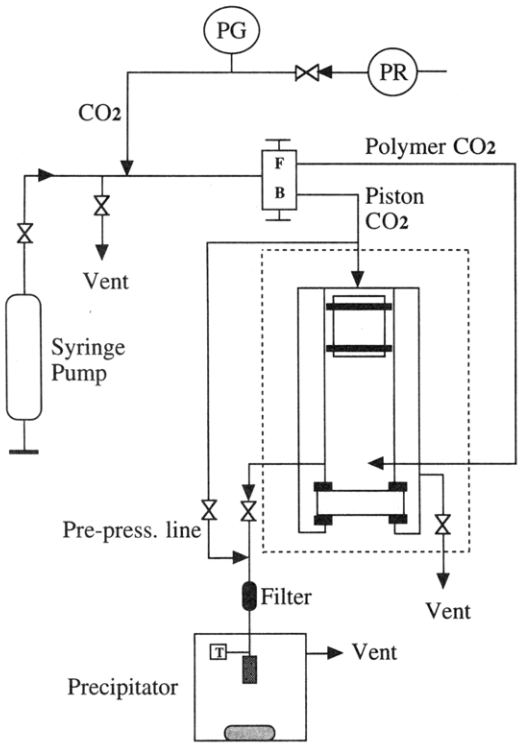


**Figure 1.** Schematic of the variable-volume cell apparatus used for poly(TA-N)/$CO_2$ phase behavior and RESS experiments.

Cloud points were observed visually by shining a light into the view cell and noting when phase separation occurred as the pressure was slowly reduced at 1−2 psig/s. In this and previous studies, the cloud point is defined as the point where fluid → liquid + liquid phase separation begins.[8,39] We defined phase separation by the point when a light, directed into the view cell, no longer reflected off the smooth stainless steel face of the piston as the solution turned slightly translucent. Meilchen et al.[16] defined the cloud point as the point at which it is no longer possible to observe the stir bar. The difference between the initial onset of phase separation and complete turbidity was observed to be within ±3−5 bar for all reported conditions and will clearly be a function of the molar mass distribution of the sample. Each cloud point condition was repeated several times with a reproducibility within ±2 bar.

Because poly(TA-N) is semicrystalline, a significant amount of time is required for initial dissolution, i.e., >10 min. Precipitates formed after initial dissolution redissolve readily. Therefore, to reproduce consistent cloud point measurements, the pressure of the polymer solution was increased >10 bar above the cloud point and the solution was agitated for 5 min until the view cell became transparent. After 5 min, agitation was stopped and the solution depressurized to determine a new cloud point.

For RESS experiments, a 10 in. long by 1/16 in. o.d. and 0.030 in. i.d. line connected the view cell to a valve (Figure 1). A preheater assembly (0.030 in. i.d. and 8 in. long) was connected to the outlet of the valve to achieve the desired pre-expansion conditions. A 2 μm frit filter was placed in the preheater line to prevent plugging of the expansion nozzle. In addition, a line was installed to prepressurize the preheater assembly with pure $CO_2$ before each spray. Otherwise, the initial pressure drop across the frit would precipitate poly(TA-N) and plug the orifice. The preheater assembly was wrapped with heavily insulated high-temperature heating tape (Omega). The solution was usually heated to above the solvent critical temperature to prevent condensation of solvent, which could produce undesirable capillary forces.[10] The pre-expansion temperature was measured with a type J thermocouple and controlled to within 0.1 °C with an Omega CN76000 temperature controller. To maintain accurate pre-expansion temperatures, the thermocouple was fitted directly into the solution stream approximately 1 cm above the entry region of the expansion nozzle. After displacing the pure $CO_2$ from the preheater, a poly(TA-N) sample was collected by directly spraying particles onto a SEM stage containing double−sided sticky tape.

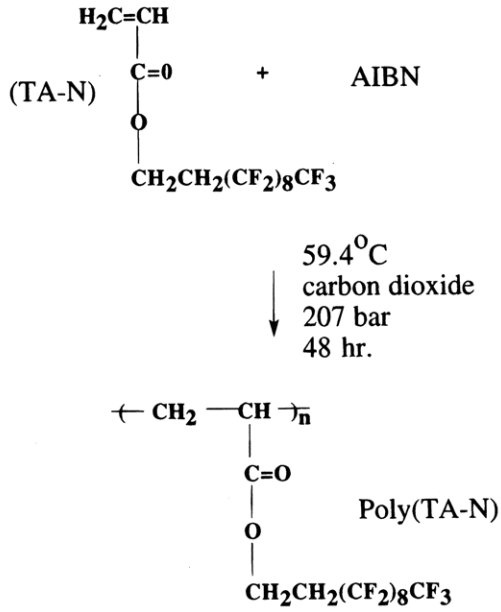


**Figure 2.** Free-radical polymerization of TA-N monomer in $CO_2$ to form semicrystalline poly(TA-N).[18]

The first expansion nozzle was a 50 μm i.d. polyimide-coated, fused-silica capillary, 1 in. long ($L/D \sim 508$). It was encased in PEEK tubing (1/16 in. o.d. and 0.010 in. i.d.) and clamped with a HIP 1/16 in. gland nut and ferrule. The second nozzle was a 0.254 mm thick, 30 μm laser-drilled orifice ($L/D \sim 8.5$), which was placed between two copper gaskets (10 mm o.d., 6 mm i.d. and 1 mm thick) and sealed in a 1/4 in. tubing assembly. The downstream end of the cap was counterbored into a V-shape to prevent the expanding jet from hitting the walls and distorting the morphology of the precipitating solute. Prior to each set of experiments, the capillary or orifice was examined under a microscope to ensure they were clean.

**Materials.** The fluoropolymer poly(1,1,2,2-tetrahydroperfluorodecyl acrylate) or poly(TA-N) was synthesized in a view cell by homogeneous solution free-radical polymerization of the TA-N monomer with AIBN initator, in $CO_2$ for 48 h at 60 °C and 207 bars as shown in Figure 2.[21] Upon completion of the polymerization, the polymer was precipitated from the $CO_2$ directly into a methanol bath via a RESS process. Once precipitated, the poly(TA-N) was washed several times and allowed to dry overnight. Analysis of the poly(TA-N) by differential scanning calorimetry indicated a melting temperature of 88 °C and no discernible $T_g$ down to 0 °C. TA-N is the trade name of the acrylate monomer produced by DuPont. The fluorocarbon ester is made through the telomerization of tetrafluoroethylene (TFE) followed by capping of 1 equiv of ethylene side chain, which allows the poly(TA-N) to crystallize. The $CO_2$ was purchased from Liquid Carbonics (bone-dry grade 99.9%).

**Characterization.** Poly(TA-N) particles and fibers were analyzed with a JEOL JSM-35C scanning electron microscope. Samples were sputter coated with gold−palladium to a thickness of approximately 200 Å. A Seiko differential scanning calorimeter (DSC) was used to determine the $T_g$ and the $T_m$ of the poly(TA-N) samples.

## Results

**Phase Behavior.** Figure 3 shows fluid → liquid + liquid (LL) phase separation at the lower critical solution temperature (LCST). This type of phase separation is characterized by an increase in the pressure with temperature, i.e., $(\partial P/\partial T)_x > 0$ and plays a key role in systems with supercritical fluid solvents. The LCST

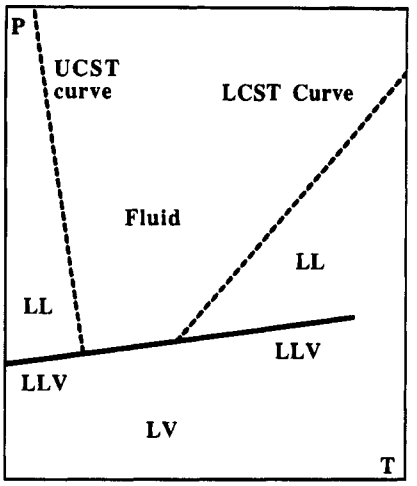


**Figure 3.** LCST phase behavior for a polymer–SCF solution.[38]

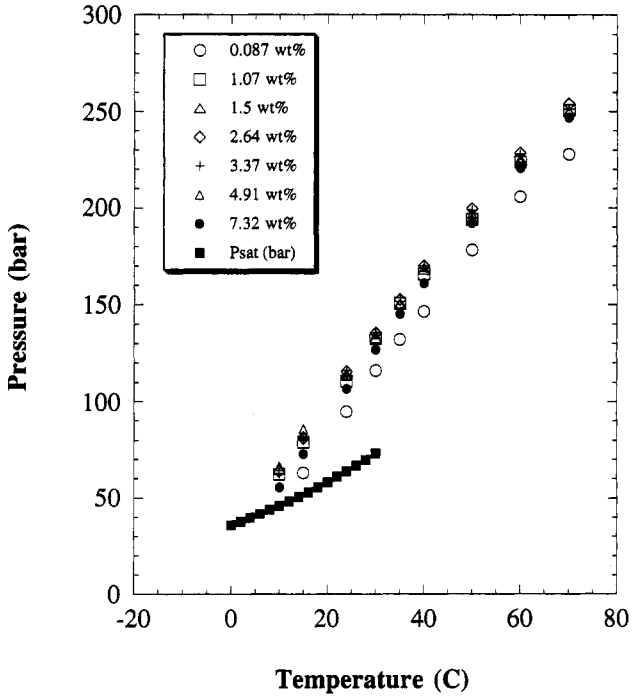


**Figure 4.** Experimental poly(TA-N) cloud point behavior in $CO_2$.

curve shown in Figure 3 may be constructed from a series of cloud point isotherms. For a given temperature and concentration, the cloud point pressure depends upon the molecular weight distribution of the polymer.[40–42]

Figure 4 shows the experimental LL cloud point curves determined for poly(TA-N) concentrations ranging from 0.087 to 7.32 wt %. The vapor pressure curve for pure carbon dioxide is also shown. At lower temperatures, the cloud point slope, $(\partial P/\partial T)_x$, varies from 3.01 to 3.21 bar/°C. Cloud point slopes for polyisobutylene in a variety of solvents, such as propane, butane, and hexane, are known to range from 1.64 to 3.03 bar/°C.[43] Poly(methyl methacrylate) cloud point slopes in chlorodifluoromethane (CDFM) are also reported around 2.8 bar/°C.[39]

Figures 5 and 6 show several temperature–concentration isobars ($T$–$x$ diagram) and pressure–concentration isotherms ($P$–$x$ diagram), respectively. It appears that the critical point (LCST or upper critical solution

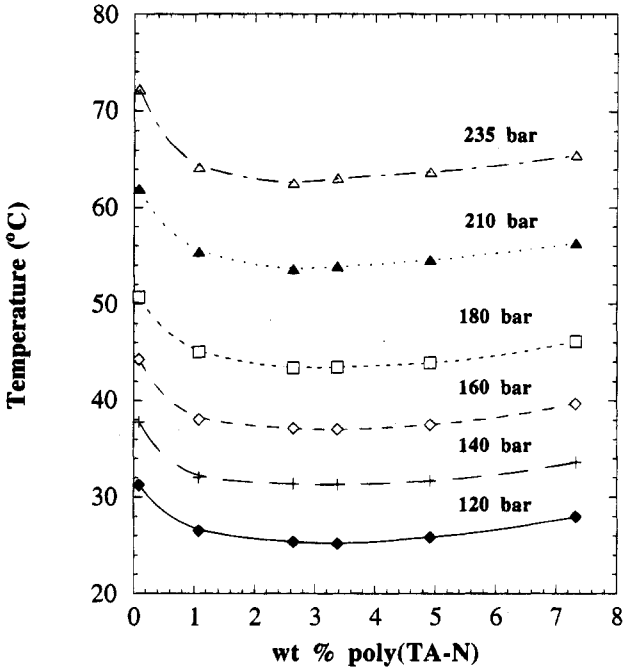


**Figure 5.** Experimental poly(TA-N)/$CO_2$ isobars showing lower critical solution temperature phase behavior. The curves connect the experimental data.

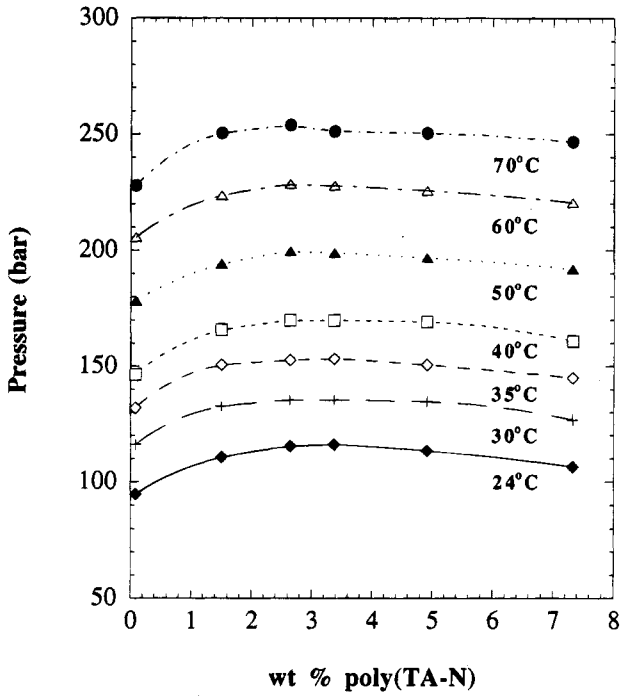


**Figure 6.** Experimental poly(TA-N) $P$–$x$ isotherms showing upper critical solution pressure phase behavior. The curves connect the experimental data.

pressure) is between 1.5 and 5.0 wt % poly(TA-N) in each case, although determination of an exact critical concentration is difficult due to the flatness of the isobar or isotherm. The curves are similar in shape for all temperatures studied. For all poly(TA-N) concentrations, the pressure necessary to maintain the poly(TA-N) solution in the one-phase region is observed to increase for increasing temperatures. The increase in pressure is needed to maintain a high solvent density.

The poly(TA-N)/$CO_2$ cloud point behavior is typical for polymer–supercritical fluid systems.[16,39,44] The occurrence of a LCST is a consequence of the large

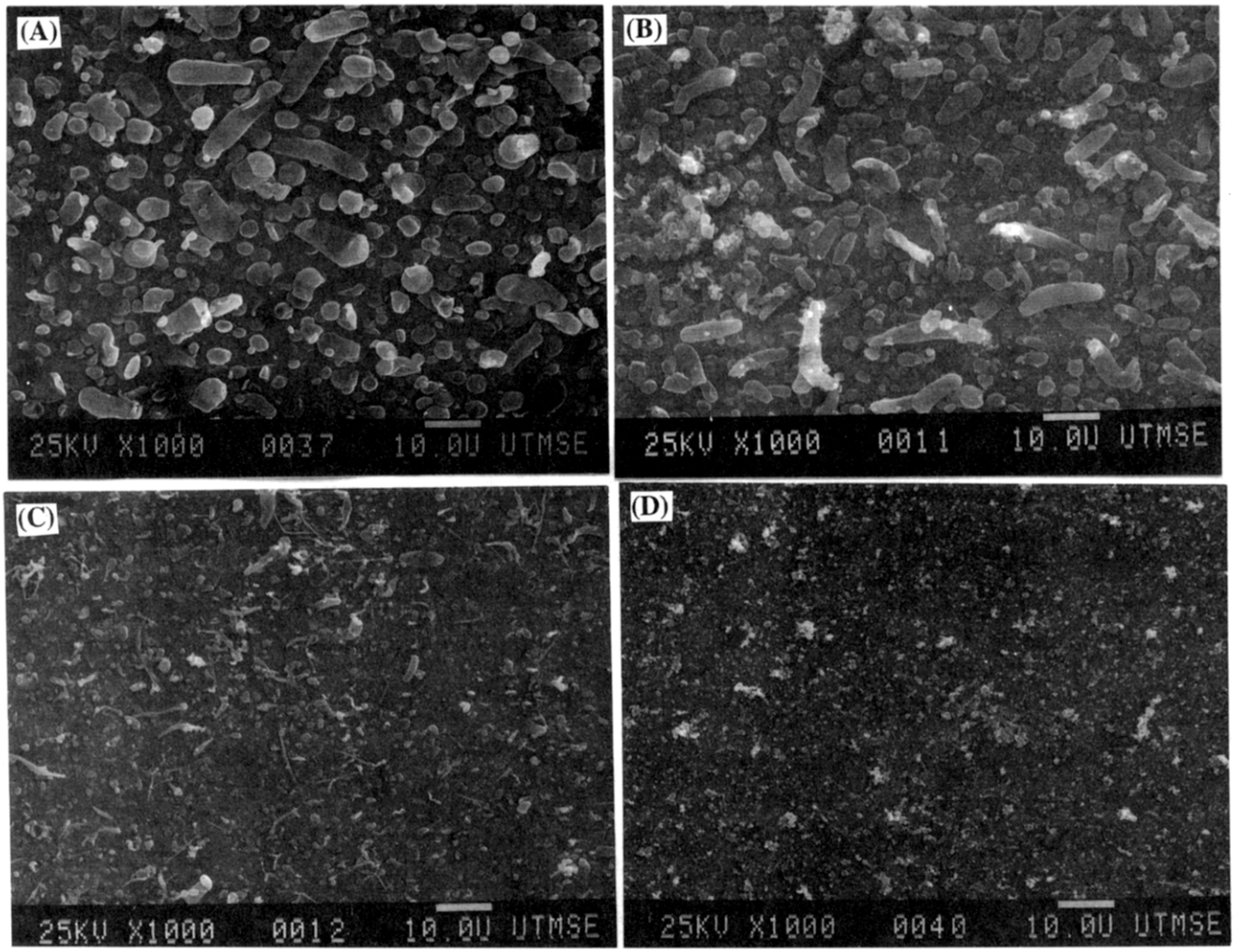


**Figure 7.** Poly(TA-N) microparticles collected from the RESS of a 0.5 wt % poly(TA-N)/$CO_2$ solution sprayed through a 30 $\mu$m orifice at pre-expansion temperatures of (A) 105, (B) 85, (C) 65, and (D) 45 °C.

difference between the free volume or thermal expansion coefficient of poly(TA-N) and the highly compressible $CO_2$.[45,46] Because $CO_2$ is more compressible than poly(TA-N), an increase in temperature or decrease in pressure will cause a larger expansion of $CO_2$ than the polymer.

When the $CO_2$ expands, it gains free volume. This results in an increase in the poly(TA-N)–poly(TA-N) segmental interactions due to localized densification. By leaving the polymer segments, $CO_2$ can expand into a new phase increasing the volume and entropy of the mixture. Therefore, at the phase separation temperature or cloud point curve, the solution free energy is minimized by an entropically driven phase separation which results in the formation of a poly(TA-N)-rich phase and a $CO_2$-rich phase. A tie line drawn on any isobar on the $T$–$x$ diagram for a 2.0 wt % poly(TA-N) solution reveals that both phases contain >90 wt % $CO_2$. Therefore, we will refer to the more viscous phase as the poly(TA-N)-enriched phase, since it is still primarily $CO_2$.

Poly(TA-N) does not form a solid phase in the presence of $CO_2$, despite a melting point of 88 °C. A homogeneous 8.85 wt % poly(TA-N) solution was isobarically cooled from 80 °C down to 24 °C at 300 bar. No phase separation was observed. Phase separation during isobaric cooling would indicate the presence of a SL transition of a depressed $T_m$.[16,17] Thermodynamically, the lack of SL phase separation is consistent with the large amount of $CO_2$ in the poly(TA-N)-enriched phase in Figure 5.[47,48] The high affinity of $CO_2$ for the fluorinated brushes is due to the low cohesive energy density of the polymer.[23–25] The interaction between $CO_2$ and the fluorocarbon brushes are likely due to van der Waals forces, as FTIR spectroscopy does not appear to provide evidence of any specific forces.[49] The $CO_2$–fluorocarbon interactions reduce the tendency of the fluorocarbon brushes to crystallize. The Lewis acid–base interactions between $CO_2$ (electron acceptor) and the acrylate (electron donor) backbone may also be important, based on the relatively high solubility of acrylate oligomers in $CO_2$.[26]

The relative amount of $CO_2$ present in the poly(TA-N)-enriched phase has a pronounced effect on the viscosity. The viscosity of the initial undissolved poly(TA-N) crystals was sufficiently high that it was not possible to agitate the stir bar. However, after dissolving the polymer and precipitating a poly(TA-N)-enriched phase, it was easy to spin the stir bar. When the pressure above this liquid phase was continually decreased, a rise in the solution viscosity was noticeable, due to loss of $CO_2$. For poly(TA-N) concentrations of 5.0 wt % and above, the crystals dissolved very slowly. However, dissolution became much more rapid when the temperature was heated near the depressed melting point. Clearly, $CO_2$ diffuses into amorphous domains more rapidly and to a greater extent than into crystalline domains.

**Table 2: Flowrate and Pressure Drop Results for Poly(TA-N)/$CO_2$ RESS Process**

| nozzle design | $T_{pre}$ (°C) | $CO_2$ flowrate (L/min STP) | $\Delta P$ (bar) |
|---|---|---|---|
| capillary | 105 | 2.2 ± 0.3 | <1.0 |
| capillary | 85 | 2.5 ± 0.3 | <1.0 |
| capillary | 65 | 2.9 ± 0.3 | <1.5 |
| capillary | 45 | 3.2 ± 0.3 | <2.0 |
| orifice | 105 | 1.5 ± 0.3 | <1.0 |
| orifice | 85 | 2.2 ± 0.3 | <1.0 |
| orifice | 65 | 2.5 ± 0.3 | <1.5 |
| orifice | 45 | 2.7 ± 0.3 | <2.0 |

**Table 3. Poly(TA-N) RESS Sprays and Resulting Morphology for a Constant Solution Temperature and Pressure of 24 °C and 207 bar**

| Figure | $L/D$ | $T_{pre}$ (°C) | conc (wt %) | $\Delta T$ (°C) | morphology |
|---|---|---|---|---|---|
| 7A | 8.5 | 105 | 0.5 | 48 | 0.5–5.0 μm particles/10 μm elongated particles (EP) |
| 7B | 8.5 | 85 | 0.5 | 28 | 0.5–3.0 μm particles, 10 μm EP |
| 7C | 8.5 | 65 | 0.5 | 8.4 | 1.0–2.0 μm spheres/larger 10 μm fibers and EP |
| 7D | 8.5 | 45 | 0.5 | −12 | <0.5 μm particles |
| 8A | 8.5 | 105 | 2.0 | 52 | 50+ μm elongates spheres (ES), 0.5–5.0 μm particles |
| 8B | 8.5 | 85 | 2.0 | 32 | 50+ μm ES, 0.5–3.0 μm particles |
| 8C | 8.5 | 65 | 2.0 | 12 | 0.5–2.0 μm particles/10+ μm ES and fibers |
| 8D | 8.5 | 45 | 2.0 | −7.7 | <1.0 μm particles |
| 9A | 508 | 105 | 0.5 | 48 | 0.3–1.0 μm fibers, 0.5–10 μm heads and particles |
| 9B | 508 | 85 | 0.5 | 28 | 0.5–1.0 μm fibers |
| 9C | 508 | 65 | 0.5 | 8.4 | <1.0 μm fibers and broken fibers |
| 9D | 508 | 45 | 0.5 | −12 | <1 μm particles and larger clusters |
| NA | 508 | 85 | 2.0 | 32 | 0.5–20 μm fibers/0.5–10 μm heads and particles |
| NA | 508 | 65 | 2.0 | 12 | 0.5–2.0 μm fibers |
| NA | 508 | 45 | 2.0 | −7.7 | 0.3–2.0 μm fibers |
| NA | 508 | 30 | 2.0 | −23 | <1.0 μm fibers/broken fibers |

**Rapid Expansion from Supercritical Solution (RESS).** The solution temperature and pressure were maintained at 24 °C and 206 bar, respectively, for all of the RESS experiments. Separate experiments were performed to determine flow rates and pressure drops as shown in Table 2. The pre-expansion temperature was varied from 105 to 45 °C at a pressure of 206 bar. The corresponding $CO_2$ flowrates upon expansion ranged from 1.5 to 3.2 ± 0.3 L/min STP. Table 2 illustrates slightly higher flowrates are observed for the 50 μm capillary expansion nozzle versus the orifice at the same pre-expansion conditions. The pressure drop from the view cell to a point 1 cm upstream of the expansion nozzle was measured to be a maximum of 2.0 bar.

A summary of the poly(TA-N) RESS experiments is presented in Table 3. To interpret the results, we define a $\Delta T$ as the difference between the pre-expansion temperature and the cloud point temperature (CP), i.e., $\Delta T = T_{(\text{pre-expansion})} - T_{CP}$. The cloud point is obtained from the $T$–$x$ phase diagram in Figure 5 at the same pressure by linear interpolation between concentrations. This property, $\Delta T$, provides a relative scale for the driving force for phase separation. For a $\Delta T$ of 0, the solution is at the phase boundary at the inlet to the nozzle. For a positive $\Delta T$ (above CP), the solution is already in the two-phase region. For a negative $\Delta T$ (below CP), the solution starts in the one-phase region. The more negative the value, the further the solution is from precipitation. Along the axis of the nozzle, the pressure and temperature change in a complex manner; thus we will not attempt to define any changes in $\Delta T$ beyond the value in the preheater.

Figure 7 shows SEM micrographs of poly(TA-N) resulting from the expansion of 0.5 wt % poly(TA-N)/$CO_2$ solution across a 30 μm orifice ($L/D$ = 8.5) for several values of $\Delta T$. For a $\Delta T$ of 48 °C in the two-phase region (Figure 7A), particles are formed which range in size from 0.5 to 5.0 μm with an average particle size of 3.0 μm. Larger elongated particles are also present with lengths up to 10 μm. Figure 7B reveals that decreasing $\Delta T$ to 28 °C decreases particle size slightly. Decreasing $\Delta T$ to 8.4 and −12 °C as shown in Figure 7C and 7D, respectively, reduces the particle size substantially. At a $\Delta T$ of 8.4 °C, the average particle size is between 1.0 and 2.0 μm with an occasional large 10 μm particle, whereas at a $\Delta T$ of −12 °C, the average particle size is <0.5 μm with no large particles present.

Increasing the concentration of the solution from 0.5 to 2.0 wt % increases the particle sizes as shown in Figure 8. Few if any previous RESS studies have considered such a high concentration. At a $\Delta T$ of 52 °C, Figure 8A reveals a substantial amount of elongated particles with lengths in excess of 50 μm and diameters up to 10 μm. These elongated spheres are dispersed among smaller 0.5–5.0 μm particles, similar to those found in Figure 7A. When the $\Delta T$ is decreased to 32 °C, as shown in Figure 8B, a modest decrease in particle size is apparent. When the $\Delta T$ is decreased further to 12 and −7.7 °C as shown in Figure 8C and 8D, respectively, there is a pronounced change in particle shape and size. At a $\Delta T$ of 12 °C, the elongated particles have much smaller diameters. At a $\Delta T$ of −7.7 °C, submicron particles are formed without any elongated particles present as is also the case for the 0.5 wt % solution shown in Figure 7D.

As shown in Figure 9, a profound change in morphology from particles to fibers takes place when the orifice ($L/D$ = 8.5) is replaced by the 50 μm capillary ($L/D$ = 508) for a 0.5 wt % solution. For a $\Delta T$ of 48 °C (Figure 9A), the morphology is primarily 0.3–1.0 μm fibers which in some instances have elongated tails flowing from a spherical head. Very few particles are present. When the $\Delta T$ is lowered to 28 and 8.4 °C, as shown in Figures 9B and 9C, respectively, the spherical heads attached to the fibrils are no longer present. At these conditions, the precipitate is predominantly 1 μm and smaller fibers. The fibers collected at a $\Delta T$ of 8.4 °C are much finer than those collected at a $\Delta T$ of 28 °C. A close look at Figure 9C reveals that a small number of the 1 μm particles are beginning to break up into particles. When the $\Delta T$ is dropped to −12 °C, the fibrous morphology is replaced with submicron poly(TA-N) particles ranging in size from 0.5 to 10 μm flocculated clusters.

For the same capillary nozzle, results are presented in Table 3 for a higher concentration of 2.0 wt %. For the three highest temperatures, the micrographs look nearly identical to those for the three highest temperatures in Figures 9A, 9B, and 9C, respectively. Essentially, no particles are observed for the two middle values of $\Delta T$, unlike previous cases which report particles accompanying all fibrous precipitate.[6,8] At a $\Delta T$ of −7.7 °C, fibers are still produced; however, they appear to be much finer and less rigid than the fibers collected at a $\Delta T$ of 12 °C. For the lower concentration of 0.5 wt % and a $\Delta T$ of −11.6 °C, recall that a transition was observed from fibers to particles for Figure 8D. In an attempt to find this transition for a concentration of 2.0 wt %, $\Delta T$ was reduced to −23 °C. As shown in Figure 9, microfibers are still produced; however, the

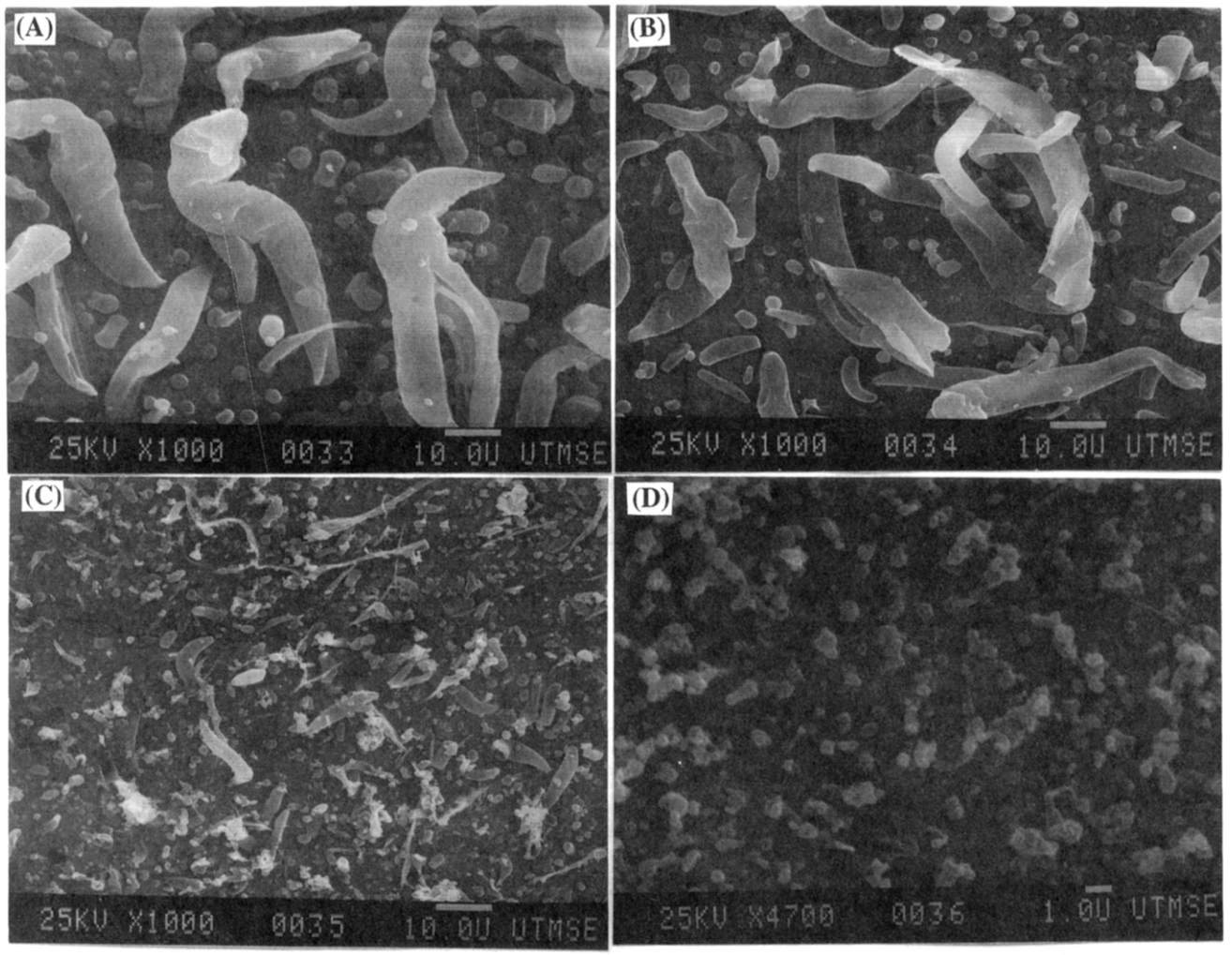


**Figure 8.** Poly(TA-N) microparticles collected from the RESS of a 2.0 wt % poly(TA-N)/$CO_2$ solution sprayed through a 30 $\mu$m orifice at pre-expansion temperatures of (A) 105, (B) 85, (C) 65, and (D) 45 °C.

fibers did appear to be shorter and to contain more spherical domains signaling the onset of a fiber to particle transition.

## Discussion

**Particle Formation Mechanism.** When a poly(TA-N) solution is expanded along the nozzle, the cohesive energy density of the solvent decreases, and LL phase separation begins at the solution cloud point curve. Due to the rapid characteristic time scale for supersaturation in the RESS process, i.e., between $10^{-5}$ and $10^{-7}$ s, a large number of polymer-enriched domains nucleate within a $CO_2$-rich continuum. For the RESS expansion of solute phenanthrene in supercritical $CO_2$, the critical domain size has been predicted to be approximately 20 nm.[12]

When the pre-expansion temperature is sufficiently high such that $\Delta T > 0$, the poly(TA-N) solution will phase separate in the preheater before it reaches the entry region of the orifice. At these conditions, thermally induced phase separation is typically on a time scale of 10 s, which is much slower than the mechanical expansion. As a result, the nuclei will grow and coalesce to much larger sizes than 100 nm as shown for the 0.5 wt % solution in Figures 7A and 7B and the 2.0 wt % poly(TA-N) solution in Figures 8A and 8B. Figures 8A and 8B also illustrate that the majority of the poly(TA-N) mass is contained in the form of >50 $\mu$m particles, with a smaller amount of 1−4 $\mu$m particles. The smaller 1−4 $\mu$m particles are similar to the particles collected for a $\Delta T$ closer to zero or even negative, which indicates that they precipitate further down the expansion nozzle. It is likely that these particles may have precipitated from the $CO_2$-rich phase, whereas the larger particles grew from the poly(TA-N)-enriched phase.

When $\Delta T$ is 0, phase separation will begin at the entrance region of the orifice. As a result, the poly(TA-N) nuclei will have less time to grow and coalesce before solidification, as is evident in Figures 7C and 8C relative to Figures 7B and 8B. In addition, the majority of the poly(TA-N) precipitate is in the form of the smaller 1−4 $\mu$m particles, not the larger 10 $\mu$m particles. A further increase in the cohesive energy density of the solution with a reduction in temperature, such that $\Delta T$ is well below zero, further delays precipitation of the poly(TA-N) solution well into the nozzle. Little time is left for growth such that small submicron particles are formed in Figures 7D and 8D.

Figure 6 shows that for an isothermal expansion process, poly(TA-N) solutions with concentrations between 1.5 and 5.0 wt % phase separate at higher pressures than for a concentration of 0.5 wt %. As a result, the solution will precipitate sooner for a concentration of 2.0 wt % relative to 0.5 wt %. Furthermore, a greater volume of poly(TA-N)-enriched domains will be present at 2.0 wt % and the chains will be more entangled. These factors will promote more growth and coalescence, which in turn produces larger particles, as

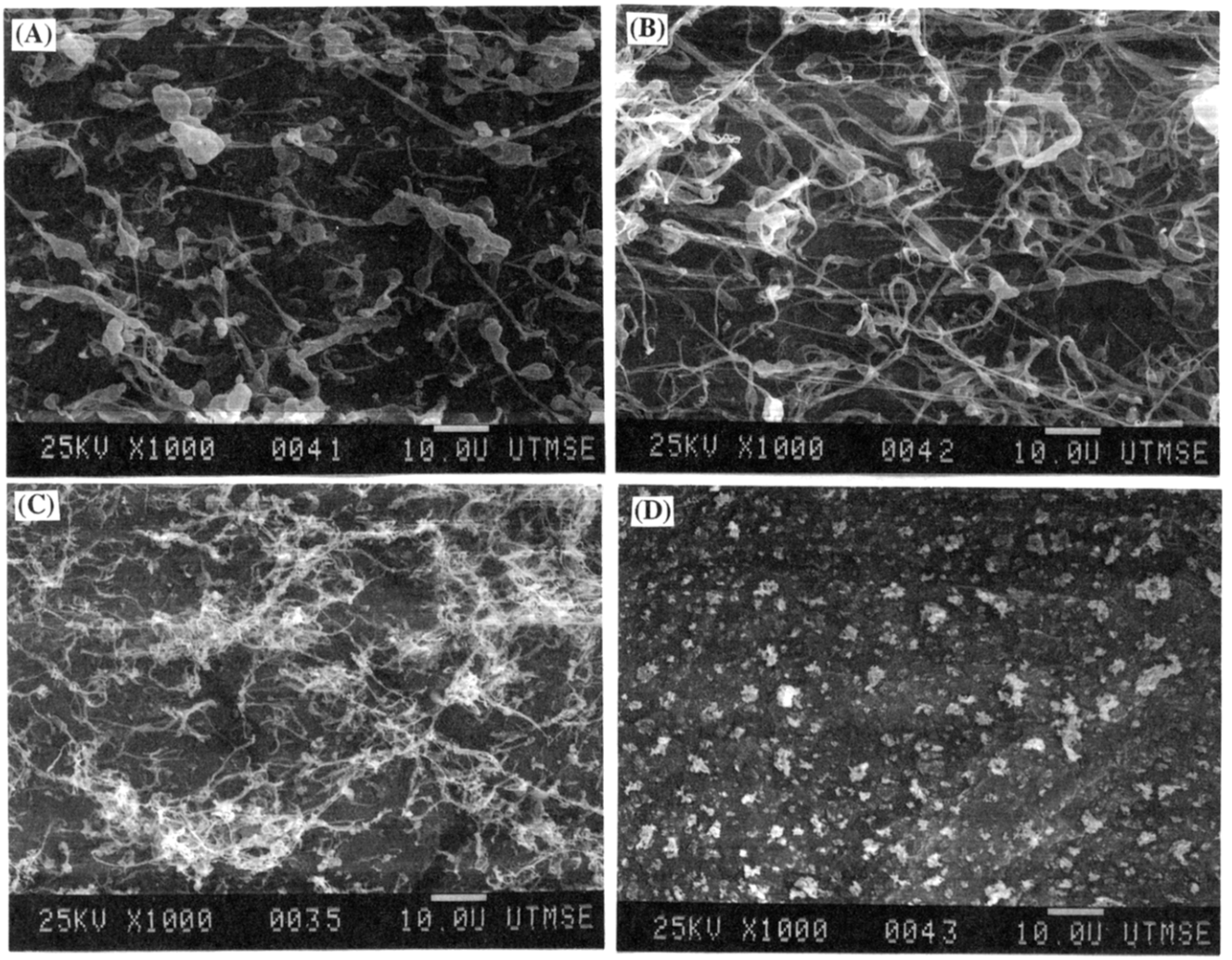


**Figure 9.** Poly(TA-N) microparticles collected from the RESS of a 0.5 wt % poly(TA-N)/$CO_2$ solution sprayed through a 50 $\mu$m capillary at pre-expansion temperatures of (A) 105, (B) 85, (C) 65, and (D) 45 °C.

is clearly evident when Figures 7A and 7B are compared with Figures 8A and 8B.

As mentioned previously, the characteristic times for phase separation in RESS and PCA are approximately $10^{-7}$ and $10^{-5}$ s, respectively. Therefore, RESS would be expected to produce smaller materials. However, the smallest poly(TA-N) particles produced (at a $T_{pre}$ = 45 °C) are around 100 nm. These materials are the same size as polystyrene particles precipitated by Dixon et al.[29] using PCA. Therefore, from particle size analysis it appears that the characteristic time for phase separation in RESS is significantly slower than theoretical predictions suggest.

For the RESS process, Berends[50] suggests that a significant pressure drop occurs in the entry region of the expansion nozzle due to streamline contraction. The pressure drop can lower solubility and enhance significantly the time for nucleation and growth. In order to show the effects of streamline contraction, experiments were performed with a sintered porous frit with 2.0 $\mu$m pores and a 62 $\mu$m single-hole orifice. As the sintered porous frit contains a multitude of 2.0 $\mu$m pathways, the effect of streamlining was reduced. When using the frit orifice, the average particle size of benzoic acid crystals precipitated from $CO_2$ was reduced from >5 $\mu$m to <1 $\mu$m.[50] These results suggest streamline contraction influences the particle size distribution in RESS.

**Fiber Formation Mechanism.** Early studies of fiber formation by RESS considered LS phase separation behavior for semicrystalline polymers such as polypropylene.[11] The pre-expansion temperature was well above $T_m$. The high pre-expansion temperatures cause the polymer to precipitate as a highly deformable melt. As a result, the polymer domains are easily deformed into fibers, with diameters ranging from 2 to 7 $\mu$m.[2,11] In the present study, much smaller fibers are formed; however, it is difficult to compare the mechanisms, as the phase behavior was not reported for the earlier study.

Lele and Shine[6] showed that amorphous PMMA expanded from a CDFM solution through a 50 $\mu$m diameter orifice produces a fibrous precipitate at pre-expansion temperatures 15 °C below the normal polymer $T_g$.[6] Further investigation has shown that the PMMA/CDFM system exhibits LL phase separation.[39] The dissolved CDFM in the PMMA-rich phase depresses the PMMA $T_g$ below the pre-expansion temperature, based on measured values of $T_g$ depressions for a weaker solvent, $CO_2$.[51,52] The plasticized PMMA was then deformed by shear forces caused by the expanding jet. Shear is widely cited as the sole mechanism for fiber formation in RESS; however, extensional forces can also contribute to chain alignment within the capillary, especially in the entrance region.[53]

For poly(TA-N), all of the experiments were well above $T_g$. However, long fibers were not formed at any values of $\Delta T$ for the 30 $\mu$m orifice. Perhaps the polymer-enriched domains were less deformable because of the

higher concentrations and lower temperatures. With the capillary nozzle which had a *L/D* of ~508, phase separation occurred well before the free jet for all $\Delta T$ values. The large velocity gradient in the long capillary sheared the poly(TA-N)-enriched drops into fibers in all cases except for a $\Delta T$ of −12 °C for the lower concentration of 0.5 wt %.

For the highest $\Delta T$ at each concentration, particles with and without 0.5−3 μm tails are formed for both concentrations. Here two phases are present in the preheater. It is likely that the poly(TA-N)-enriched domains were sufficiently large at this point that they could not be totally sheared into fibers in the capillary. Because of the high temperature, the viscosity or the shearing ability of the expanding $CO_2$ was also reduced, making it more difficult to deform the poly(TA-N)-rich drops. At 100 bar, the viscosity decreases almost 50% from 75.5 to 36.9 μPa s as the temperature is raised from 45 to 105 °C.[54] As a result, the particle to fiber deformation started but was only partially completed. The small amount of 1−4 μm particles which accompany the fibers are similar to the small particles which accompanied the larger particles expanded through the orifice at similar conditions. Again, these particles could result from the residual poly(TA-N) in the $CO_2$-rich phase.

For smaller values of $\Delta T$ in the range of 8.4−12 °C, fibers are formed with diameters of 0.5−2.0 μm and aspect ratios >100. In addition, a certain amount of orientation in some of the fibers is also evident. At these conditions, all of the poly(TA-N) is sheared into fibers and no particles are formed. In contrast, large numbers of particles were always present with the fibers in previous studies as the much smaller *L/D* did not allow for enough time for the particles to coalesce and be sheared into fibers.[6,8] Furthermore, the concentrations were lower.

If solute nucleation were prevented until the exit region of the expansion nozzle, then the capillary will imitate a small *L/D* orifice. Rather than observing fibers, it should be possible to form particles as the deformation forces become insignificant. This fiber to particle transition was achieved for a $\Delta T$ of −12 °C at 0.5 wt % but was not found even for a $\Delta T$ of −23 °C at 2.0 wt %. The higher concentration favors fiber formation due to greater entanglement and greater coalescence from collisions between polymer-enriched domains.

From the DSC analysis, the $T_g$ of poly(TA-N) has been determined to be −23.3 °C. Because crystal growth occurs between $T_g$ and $T_m$, it is difficult to determine how much crystallization occurs during the expansion process versus during depressurization and transfer to the DSC. Comparisons of DSC scans of 5.0 wt % RESS poly(TA-N) fibers and the original poly(TA-N) reveal that both samples contain the same amount of crystalline polymer. As crystallinity occurs in oriented polymers more easily than in unoriented polymers, it is highly probable that the poly(TA-N) chains are initially sheared into oriented crystalline domains.[6] After the expansion process, the remaining amorphous poly(TA-N) matrix crystallizes as evidenced by the similarity of the DSC melting endotherms.

## Conclusions

The cloud point experiments indicate LCST phase behavior for the poly(TA-N)/$CO_2$ system with LL phase separation, and no SL phase separation down to 24 °C. The interactions between the fluorocarbon grafts and $CO_2$ are sufficiently favorable to prevent any low-temperature infringement of a SL crystallization phase transition on the LL cloud point curve. The Lewis acidity of $CO_2$ may also play a role in the interactions with the acrylate groups.

Rapid expansion from supercritical solution (RESS) of poly(TA-N) produces 0.3−50 μm particles and 0.3−2.0 μm fibers. Unlike a previous study, no particles were mixed with the fibers at higher concentrations, because the *L/D* was 2 orders of magnitude larger.[8] To our knowledge, submicron fibers by RESS have not been shown previously.

The understanding of the RESS mechanism has been clarified by careful design of experimental variables and procedures. It turns out to be very important to know the inlet solution concentration and to hold it constant, so that the morphology can be related to $\Delta T$ ($\Delta T = T_{(\text{pre-expansion})} - T_{CP}$), which affects the location of phase separation in the nozzle.

The results provide clear evidence to support the mechanism of Lele and Shine.[6] The earlier the phase separation in the nozzle, the greater the time for coalescence and fiber formation of the polymer-enriched nuclei. The *L/D* is the most influential variable for achieving a transition from particles or fibers. Usually, particles were produced with the orifice and fibers were produced with the capillary nozzle. In most cases, the solution concentration and the pre-expansion temperature did not produce this transition, but the sizes of the particles and fibers decreased significantly as the temperature was lowered ($\Delta T$ decreased).

When $T_{pre} > T_{CP}$ ($\Delta T > 0$), thermally induced phase separation occurs early in the expansion. For the orifice, large elongated particles were observed, indicating ample time for growth and coalescence but only a short time for shear. Few fibers were formed. The capillary nozzle produced a mixture of fibers and particles with and without drawn-out tails. The shear was insufficient to convert all of the particles totally to fibers because of the low viscosity of $CO_2$ at high temperatures.

As the temperature was reduced such that $T_{pre} \leq T_{CP}$ ($\Delta T \leq 0$), the sizes of the particles and fibers decreased due to later phase separation. The concentration of the solution was found to have a secondary effect on the sizes of the precipitated materials, which is consistent with the flatness of the cloud point curves. At certain values of $\Delta T$, the fibers formed in the capillary nozzle were not accompanied by particles, as the *L/D* was sufficiently high to shear all poly(TA-N)-enriched nuclei into fibers. It was possible to achieve a fiber to particle transition by further delaying phase separation when $\Delta T$ was reduced to −12 °C. This transition occurred for a 0.5 wt % poly(TA-N) solution but not for a more viscous 2.0 wt % solution for a $\Delta T$ as low as −23 °C.

**Acknowledgment.** At UT, we are grateful for support from the NSF (Grant CTS-9218769), the Texas Advanced Technology Program (Grant 3658-198), and the Separations Research Program at the University of Texas. We thank Dr. Peter Condo, Gabriel Luna-Bàrcenas, and Kristi Harrison for many helpful discussions on high-pressure phase behavior. Also, support at UNC is gratefully acknowledged from the NSF through a Presidential Faculty Fellowship (J.M.D.: 1993−1994), DuPont, and 3M.

## References and Notes


(1) Krukonis, V. Supercritical Fluid Nucleation of Difficult-to-Comminute Solids, paper 104f, AIChE Fall Meeting, 1984.
(2) Matson, D. W.; Fulton, J. L.; Peterson, R. C.; Smith, R. D. *Ind. Eng. Chem. Res.* **1987**, *26*, 2298.
(3) Chang, C. J.; Randolph, A. D. *AIChE J.* **1989**, *35*, 1876.
(4) Mohamed, R. S.; Halverson, D. S.; Debenedetti, P. G.; Prud'homme, R. K. In *Supercritical Fluid Science and Technology*; Johnston, K. P., Penninger, J. M. L., Eds.; ACS Symposium Series 406; American Chemical Society: Washington, DC, 1989; p 355.
(5) Ohgaki, K.; Kobayashi, H.; Katayama, T. *J. Supercrit. Fluids* **1990**, *3*, 103.
(6) Lele, A. K.; Shine, A. D. *AIChE J.* **1992**, *38*, 742.
(7) Tom, J. W.; Debenedetti, P. G. *Biotechnol. Prog.* **1991**, *7*, 403.
(8) Lele, A. K.; Shine, A. D. *Ind. Eng. Chem. Res.* **1994**, *33*, 1476.
(9) Boen, S. N.; Bruch, M. D.; Lele, A. K.; Shine, A. D. In *Polymer Solutions, Blends, and Interfaces*; Noda, I., Rubingh, D. N., Eds.; Elsevier Science Publishers B.V.: Amsterdam, 1992; p 151.
(10) Matson, D. W.; Peterson, R. C.; Smith, R. D. *J. Mater. Sci.* **1987**, *22*, 1919.
(11) Peterson, R. C.; Matson, D. W.; Smith, R. D. *Polym. Eng. Sci.* **1987**, *27*, 1693.
(12) Debenedetti, P. G. *AIChE J.* **1990**, *36*, 1289.
(13) Debenedetti, P. G.; Tom, J. W.; Kwauk, X.; Yeo, S. D. *Fluid Phase Equilib.* **1993**, *82*, 311.
(14) Kwauk, X.; Debenedetti, P. G. *J. Aerosol. Sci.* **1993**, *24*, 445.
(15) Liang, M.; Rasmussem, D. H. *AIChE J.*, in press.
(16) Meilchen, M. A.; Hasch, B. M.; McHugh, M. A. *Macromolecules* **1991**, *24*, 4974.
(17) Condo, P. D., Jr.; Colman, E. J.; Ehrlich, P. *Macromolecules* **1992**, *25*, 750.
(18) Tom, J. W.; Debenedetti, P. G.; Jerome, R. *J. Supercrit. Fluids* **1994**, *7*, 9.
(19) Goel, S. K.; Beckman, E. J. *Polym. Eng. Sci.* **1994**, *34*, 1137.
(20) Goel, S. K.; Beckman, E. J. *Polym. Eng. Sci.* **1994**, *34*, 1148.
(21) DeSimone, J. M.; Guan, Z.; Elsbernd, C. S. *Science* **1992**, *257*, 945.
(22) Johnston, K. P. *Nature* **1994**, *368*, 187.
(23) Harrison, K. L.; Goveas, J.; Johnston, K. P.; O'Rear, E. A., III. *Langmuir* **1994**, *10*, 3536.
(24) McFann, G. J.; Johnston, K. P.; Howdle, S. M. *AIChE J.* **1994**, *40*, 543.
(25) Hoefling, T. A.; Enick, R. M.; Beckman, E. J. *J. Phys. Chem.* **1991**, *95*, 7127.
(26) McHugh, M. A.; Krukonis, V. In *Encyclopedia of Polymer Science and Engineering*, 2nd ed.; Mark, H. F., Bikales, N. M., Overberger, C. G., Menges, G., Eds.; John Wiley: New York, 1988; Vol. 16.
(27) Lele, A. K.; Shine, A. D. *Polym. Prepr. (Am. Chem. Soc., Div. Polym. Chem.)* **1991**, *31*, 677.
(28) Tom, J. W.; Debenedetti, P. G. *Polym. Prepr. (Am. Chem. Soc., Div. Polym. Chem.)* **1992**, *33*, 104.
(29) Dixon, D. J.; Bodmeier, R. A.; Johnston, K. P. *AIChE J.* **1993**, *39*, 127.
(30) Dixon, D. J. Ph.D. Thesis, The University of Texas at Austin, 1993.
(31) Yeo, S.-D.; Debenedetti, P. G.; Radosz, M.; Schmidt, H.-W. *Macromolecules* **1993**, *26*, 6207.
(32) Bàrcenas, G. L.; Kanakia, S. K.; Sanchez, I. C.; Johnston, K. P. *Polymer*, submitted.
(33) Dixon, D. J.; Johnston, K. P. *J. Appl. Polym. Sci.* **1993**, *50*, 1929.
(34) Bodmeier, R.; Wang, H.; Dixon, D. J.; Mawson, S.; Johnston, K. P. *Pharm. Res.*, submitted.
(35) Dixon, D. J.; Luna-Bárcenas, G.; Johnston, K. P. *Polymer* **1994**, *35*, 18, 3998.
(36) Nielson, K. A.; Argyropoulos, J. N.; Clark, R. C.; Goad, J. D. In Third Annual Advanced Coatings Technology Conference, Dearborn, MI, 1993.
(37) DeSimone, J. M.; Maury, E. E.; Menceloglu, Y. Z.; McClain, J. B.; Romack, T. J.; Combes, J. R. *Science* **1994**, *265*, 356.
(38) Lemert, R. M.; Fuller, R. A.; Johnston, K. P. *J. Phys. Chem.* **1994**, *94*, 6021.
(39) Haschets, C. W.; Shine, A. D. *Macromolecules* **1993**, *26*, 5052.
(40) Ehrlich, P. *Chemtracts:Macromol. Chem.* **1992**, *3*, 1.
(41) Irani, C. A. *J. Appl. Polym. Sci.* **1986**, *31*, 1879.
(42) Allen, G.; Baker, C. H. *Polymer* **1965**, *6*, 181.
(43) Zeman, L.; Biros, J.; Delmas, G.; Patterson, D. *J. Phys. Chem.* **1972**, *76*, 1206.
(44) Kiran, E.; Zhuang, W. *Polymer* **1992**, *33*, 5459.
(45) Somcynsky, T. *Polym. Eng. Sci.* **1982**, *22*, 58.
(46) Sanchez, I. C. In *Encyclopedia of Physical Science and Technology*; Academic Press: New York, 1992; Vol. 13, p 153.
(47) Lemert, R. M.; Johnston, K. P. *Fluid Phase Equilib.* **1989**, *45*, 265.
(48) McHugh, M. A.; Krukonis, V. J. *Supercritical Fluid Extraction Principles and Practice*, 2nd ed.; Butterworths: Stoneham, MA, 1994.
(49) Yee, G. G.; Fulton, J. L.; Smith, R. D. *J. Phys. Chem.* **1992**, *96*, 6172.
(50) Berends, E. M. Ph.D. Thesis, Delft Technical University, 1994.
(51) Condo, P. D.; Sanchez, I. C.; Panayiotou, C. G.; Johnston, K. P. *Macromolecules* **1992**, *25*, 6119.
(52) Condo, P. D.; Johnston, K. P. *J. Polym. Sci.; Part B: Polym. Phys.* **1992**, *32*, 523.
(53) Ziabicki, A. *Fundamentals of Fiber Formation*; John Wiley and Sons: New York, 1976.
(54) Vesovic, V.; Wakeham, W. A.; Olchowy, G. A.; Sengers, J. V.; Watson, J. T. R.; Millat, J. *J. Phys. Chem. Ref. Data* **1990**, *19*, 763.


MA946107M